Letter

Mixed configurations and intertwined quantum phase transitions in odd-mass nuclei

N. Gavrielov [1,2,*] A. Leviatan [2,†] and F. Iachello [1,‡]

[1] *Center for Theoretical Physics, Sloane Physics Laboratory, Yale University, New Haven, Connecticut 06520-8120, USA*

[2] *Racah Institute of Physics, The Hebrew University, Jerusalem 91904, Israel*

(Received 7 September 2022; accepted 10 November 2022; published 21 November 2022)

We introduce a new Bose-Fermi framework for studying spectral properties and quantum phase transitions (QPTs) in odd-mass nuclei, in the presence of configuration mixing. A detailed analysis of odd-mass Nb isotopes discloses the effects of an abrupt crossing of states in normal and intruder configurations (Type II QPT), accompanied by a gradual evolution from spherical- to deformed-core shapes within the intruder configuration (Type I QPT). The pronounced presence of both types of QPTs demonstrates, for the first time, the occurrence of intertwined QPTs in odd-mass nuclei.

DOI: 10.1103/PhysRevC.106.L051304

Structural changes induced by variation of parameters in the Hamiltonian, called quantum phase transitions (QPTs) [1,2], are salient phenomena in dynamical systems, and form the subject of ongoing intense experimental and theoretical activity in diverse fields [3]. In nuclear physics, most of the attention has been devoted to the evolution of structure with nucleon number, exhibiting two types of phase transitions. The first, denoted as Type I [4], is a shape-phase transition in a single configuration, as encountered in the neutron number 90 region [5]. The second, denoted as Type II [6], is a phase transition involving an abrupt crossing of different configurations, as encountered in nuclei near (sub)shell closures [7]. If the mixing is small, the Type II QPT can be accompanied by a distinguished Type I QPT within each configuration separately. Such a scenario, referred to as intertwined QPTs (IQPTs), was recently shown to occur in the Zr isotopes [8,9].

Most studies of QPTs in nuclei have focused on systems with even numbers of protons and neutrons [5,7,10–12]. The structure of odd-mass nuclei is more complex due to the presence of both collective and single-particle degrees of freedom. Consequently, QPTs in such nuclei have been far less studied. Fully microscopic approaches to QPTs in medium-heavy odd-mass nuclei, such as the large-scale shell model [13] and beyond-mean-field methods [14], are computationally demanding and encounter difficulties. Alternative approaches have been proposed, including algebraic modeling (shell-model inspired [15–17] and symmetry-based [18–24]) and density functionals-based mean-field methods [25–28], involving particle-core coupling schemes with boson-fermion or collective Hamiltonians. So far these approaches were restricted to Type I QPTs in odd-mass nuclei without configuration mixing.

The goals of the present Letter are twofold. (*i*) To introduce a framework for studying spectral properties and QPTs with configuration mixing, in odd-mass nuclei. This is motivated by a wealth of new experimental data on shape-coexisting states in such nuclei near shell closure [29,30], whose awaiting interpretation necessitates multiple configurations. (*ii*) To apply the formalism and show evidence for concurrent types of QPTs exemplifying, for the first time, IQPTs in odd-mass nuclei.

Odd-A nuclei are treated in the interacting boson-fermion model (IBFM) [16], as a system of monopole (s) and quadrupole (d) bosons, representing valence nucleon pairs, and a single (unpaired) nucleon. We propose to extend the IBFM to include core excitations and obtain a boson-fermion model with configuration mixing (IBFM-CM), employing a Hamiltonian of the form

$$\hat{H} = \hat{H}_{\rm b} + \hat{H}_{\rm f} + \hat{V}_{\rm bf}. \tag{1}$$

The boson part ($\hat{H}_{\rm b}$) is the Hamiltonian of the configuration mixing model (IBM-CM) of [31,32]. For two configurations (A,B), it can be cast in matrix form [6],

$$\hat{H}_{\rm b} = \begin{bmatrix} \hat{H}_{\rm b}^{\rm A}(\xi^{(\rm A)}) & \hat{W}_{\rm b}(\omega) \\ \hat{W}_{\rm b}(\omega) & \hat{H}_{\rm b}^{\rm B}(\xi^{(\rm B)}) \end{bmatrix}. \tag{2}$$

Here, $\hat{H}_{\rm b}^{\rm A}(\xi^{(\rm A)})$ represents the normal A configuration (N boson space) and $\hat{H}_{\rm b}^{\rm B}(\xi^{(\rm B)})$ represents the intruder B configuration ($N+2$ boson space), corresponding to 2p-2h excitations across the (sub)shell closure. Standard forms, as in Eq. (4) of Ref. [9], include pairing, quadrupole, and rotational terms, and a mixing term $\hat{W}_{\rm b} = \omega[(d^\dagger d^\dagger)^{(0)} + (s^\dagger)^2]$ + Hermitian conjugate (H.c.). Such IBM-CM Hamiltonians have been used extensively for the study of configuration-mixed QPTs and shape coexistence in even-even nuclei [8,9,31–39].

*noam.gavrielov@yale.edu

†ami@phys.huji.ac.il

‡francesco.iachello@yale.edu

The fermion Hamiltonian ($\hat{H}_{\rm f}$) of Eq. (1) has the form

$$\hat{H}_{\rm f} = \begin{bmatrix} \sum_j \epsilon_j^{(\rm A)} \hat{n}_j & 0 \\ 0 & \sum_j \epsilon_j^{(\rm B)} \hat{n}_j \end{bmatrix}, \tag{3}$$

where j is the angular momentum of the occupied orbit, $\hat{n}_j$ the corresponding number operator, and $\epsilon_j^{(\rm i)}$ ($i = {\rm A}, {\rm B}$) are the single-particle energies for each configuration. The boson-fermion interaction has the form

$$\hat{V}_{\rm bf} = \begin{bmatrix} \hat{V}_{\rm bf}^{\rm A}(\zeta^{(\rm A)}) & \hat{W}_{\rm bf}(\omega_j) \\ \hat{W}_{\rm bf}(\omega_j) & \hat{V}_{\rm bf}^{\rm B}(\zeta^{(\rm B)}) \end{bmatrix}. \tag{4}$$

Here, $\hat{V}_{\rm bf}^{(i)}$ ($i = {\rm A}, {\rm B}$) involve monopole, quadrupole, and exchange terms with parameters $\zeta^{(i)} = (A_j^{(i)}, \Gamma_{jj'}^{(i)}, \Lambda_{jj'}^{(i)j''})$. Using the microscopic interpretation of the IBFM [16], these couplings can be expressed in terms of strengths $(A_0^{(i)}, \Gamma_0^{(i)}, \Lambda_0^{(i)})$ and occupation probabilities (u_j, v_j). The term $\hat{W}_{\rm bf}(\omega_j) = \sum_j \omega_j \hat{n}_j [(d^\dagger \tilde{d})^{(0)} + (s^\dagger)^2 + {\rm H.c.}]$, controls the mixing for each orbit.

The Hamiltonian of Eq. (1) is diagonalized numerically. The resulting eigenstates $|\Psi; J\rangle$ are linear combinations of wave functions $\Psi_{\rm A}$ and $\Psi_{\rm B}$, involving bosonic basis states in the two spaces $|[N], \alpha, L\rangle$ and $|[N+2], \alpha, L\rangle$. The boson (L) and fermion (j) angular momenta are coupled to J, $|\Psi; J\rangle = \sum_{\alpha,L,j} C_{\alpha,L,j}^{(N,J)} |\Psi_{\rm A}; [N], \alpha, L; j; J\rangle + \sum_{\alpha,L,j} C_{L,j}^{(N+2,J)} |\Psi_{\rm B}; [N+2], \alpha, L; j; J\rangle$. The probability of normal-intruder mixing is given by

$$a^2 = \sum_{\alpha,L,j} \left| C_{\alpha,L,j}^{(N,J)} \right|^2, \quad b^2 = 1 - a^2 = \sum_{\alpha,L,j} \left| C_{\alpha,L,j}^{(N+2,J)} \right|^2. \tag{5}$$

Operators inducing electromagnetic transitions of type σ and multipolarity L contain boson and fermion parts,

$$\hat{T}(\sigma L) = \hat{T}_{\rm b}(\sigma L) + \hat{T}_{\rm f}(\sigma L). \tag{6}$$

For $E2$ transitions, $\hat{T}_{\rm b}(E2) = e^{(\rm A)} \hat{Q}_\chi^{(N)} + e^{(\rm B)} \hat{Q}_\chi^{(N+2)}$, where the superscript (N) denotes a projection onto the $[N]$ boson space and $\hat{Q}_\chi = d^\dagger s + s^\dagger \tilde{d} + \chi (d^\dagger \tilde{d})^{(2)}$. For $M1$ transitions, $\hat{T}_{\rm b}(M1) = \sum_i \sqrt{\frac{3}{4\pi}} g^{(i)} \hat{L}^{(N_i)} + \tilde{g}^{(i)} [\hat{Q}_\chi^{(N_i)} \times \hat{L}^{(N_i)}]^{(1)}$, where $i = ({\rm A}, {\rm B})$, $N_{\rm A} = N$, $N_{\rm B} = N+2$. The fermion operators $\hat{T}_{\rm f}(\sigma L)$ have the standard form [16] with effective charge e_f for $E2$ transitions, and g_s quenched by 20% for $M1$ transitions. In what follows, we apply the above IBFM-CM framework to the study of QPTs in the odd-mass Nb isotopes.

The ${}^{A}_{41}$Nb isotopes with mass number $A = 93$–105 are described by coupling a proton to their respective ${}_{40}$Zr cores with neutron number 52–64. In the latter, the normal A configuration corresponds to having no active protons above the $Z = 40$ subshell gap, and the intruder B configuration corresponds to two-proton excitation from below to above this gap, creating 2p-2h states. The parameters of $\hat{H}_{\rm b}$ (2) and boson numbers are taken to be the same as in a previous calculation of these Zr isotopes (see Table V of Ref. [9]), except for $\chi = -0.565$ at neutron number 64.

For ${}_{41}$Nb isotopes, the valence protons reside in the $Z = 28$–50 shell. Using as an input the empirical single-proton energies (taken from Table XI of Ref. [40]) and a pairing gap $\Delta_{\rm F} = 1.5$ MeV, a BCS calculation yields the single quasiparticle energies (ϵ_j) and occupation probabilities (v_j^2) for the considered $1g_{9/2}, 2p_{1/2}, 2p_{3/2}, 1f_{5/2}$ orbits, assuming, for simplicity, the same parameters for both configurations. The derived ϵ_j and v_j^2, and the common strengths $(A_0, \Gamma_0, \Lambda_0)$, obtained by a fit, are listed in Table I. As seen, the monopole term (A_0) vanishes for neutron number 52–56 and corrects the quasiparticle energies at neutron number 58–64. The quadrupole term (Γ_0) is constant for the entire chain. The exchange term (Λ_0) increases towards the neutron midshell [16]. Altogether, the values of the parameters are either constant for the entire chain or segments of it and vary smoothly. We take $\omega_j = 0$ in the $\hat{W}_{\rm bf}$ term of Eq. (4), since for equal ω_j it coincides with the $\hat{W}_{\rm b}$ term of Eq. (2).

TABLE I. Parameters in MeV of the boson-fermion interactions, $\hat{V}_{\rm bf}^{(i)}$ of Eq. (4), obtained from a fit assuming $A_0^{(i)} = A_0$, $\Gamma_0^{(i)} = \Gamma_0$ and $\Lambda_0^{(i)} = \Lambda_0$, $\epsilon_j^{(i)} = \epsilon_j$, where ($i = {\rm A}, {\rm B}$). From a BCS calculation, $\epsilon_j = 1.639$, 1.524, 2.148 and 2.519 MeV and $v_j^2 = 0.299$, 0.589, 0.858, and 0.902, for the $1g_{9/2}, 2p_{1/2}, 2p_{3/2}, 1f_{5/2}$ orbits, respectively, and Fermi energy $\lambda_F = 2.024$ MeV.

Neutron number	52	54	56	58	60	62	64
A_0	0.00	0.00	0.00	−0.11	−0.20	−0.20	−0.20
Γ_0	1.00	1.00	1.00	1.00	1.00	1.00	1.00
Λ_0	1.00	1.00	3.00	3.00	3.80	3.80	3.80

In the present Letter, we concentrate on the positive-parity states in Nb isotopes, postponing a discussion of both parity states to a longer paper. Such a case reduces to a single-j calculation, with the $\pi(1g_{9/2})$ orbit coupled to the boson core. Figure 1 shows the experimental and calculated levels of selected states, along with assignments to configurations based on Eq. (5). Open (solid) symbols indicate a dominantly normal (intruder) state with small (large) b^2 probability. In

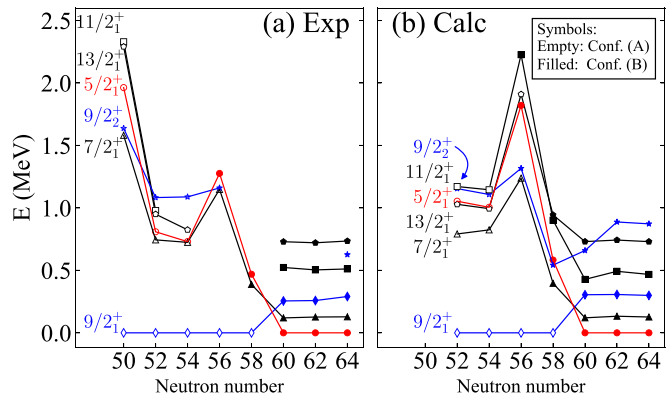

FIG. 1. Comparison between (a) experimental [41–45] and (b) calculated lowest-energy positive-parity levels in Nb isotopes. Open (solid) symbols indicate a state dominated by the normal A configuration (intruder B configuration), with assignments based on Eq. (5). In particular, the $9/2_1^+$ state is in the A (B) configuration for neutron number 52–58 (60–64) and the $5/2_1^+$ state is in the A (B) configuration for 52–54 (56–64). Note that the calculated values start at 52, while the experimental values include the closed shell at 50.

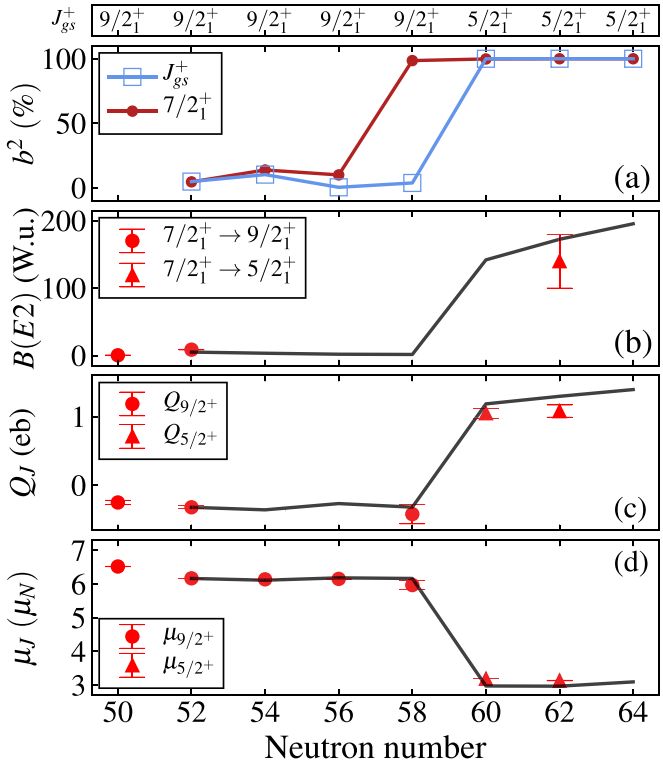

FIG. 2. Evolution of spectral properties along the Nb chain. Symbols (solid lines) denote experimental data (calculated results). (a) Percentage of the intruder (B) component [the b^2 probability in Eq. (5)], in the ground state (J^+_{gs}) and the first-excited positive-parity state ($7/2^+_1$) of $^{93-103}$Nb. The values of J^+_{gs} are indicated at the top. (b) $B(E2; 7/2^+_1 \to J^+_{gs})$ in Weisskopf units (W.u.). (c) Quadrupole moments of J^+_{gs} in eb. (d) Magnetic moments of J^+_{gs} in μ_N. Data in (b)–(d), are taken from Refs. [41,42,47], Refs. [41,42,48], and Refs. [41–45,48], respectively.

the region between neutron number 50 and 56, there appear to be two sets of levels with a weakly deformed structure, associated with configurations A and B. All levels decrease in energy for 52–54, away from the closed shell, and rise again at 56 due to the $\nu(2d_{5/2})$ subshell closure. From 58, there is a pronounced drop in energy for the states of the B configuration. At 60, the two configurations cross, indicating a Type II QPT, and the ground state changes from $9/2^+_1$ to $5/2^+_1$, becoming the bandhead of a $K = 5/2^+$ rotational band composed of $5/2^+_1, 7/2^+_1, 9/2^+_1, 11/2^+_1, 13/2^+_1$ states. The intruder B configuration remains strongly deformed and the band structure persists beyond 60. The above trend is similar to that encountered in the even-even Zr isotopes with the same neutron numbers (see Fig. 14 of Ref. [9]).

A possible change in the angular momentum of the ground state (J^+_{gs}) is a characteristic signature of Type II QPTs in odd-mass, unlike even-even nuclei where the ground state remains 0^+ after the crossing. It is an important measure for the quality of the calculations, since a mean-field approach, without configuration mixing, fails to reproduce the switch $9/2^+_1 \to 5/2^+_1$ in J^+_{gs} for the Nb isotopes [46]. Figure 2(a) shows the percentage of the wave function within the B configuration for J^+_{gs} and $7/2^+_1$, as a function of neutron number across the Nb chain. The rapid change in structure of J^+_{gs} from the normal A configuration in $^{93-99}$Nb (small b^2 probability), to the intruder B configuration in $^{101-105}$Nb (large b^2) is clearly evident, signaling a Type II QPT. The configuration change appears sooner in the $7/2^+_1$ state, which changes to the B configuration already in ^{99}Nb. Outside a narrow region near neutron number 60, where the crossing occurs, the two configurations are weakly mixed and the states retain a high level of purity. Such a trend is similar to that encountered for the 0^+_1 and 2^+_1 states in the respective $_{40}$Zr cores (see Fig. 10 of Ref. [9]).

Electromagnetic transitions and moments provide further insight into the nature of QPTs. For $\hat{T}_{\rm b}(E2)$ of Eq. (6), we adopt the same parameters $(e^{(\rm A)}, e^{(\rm B)}, \chi)$ used for the core Zr isotopes [9], with a slight modification of $e^{(\rm A)} = 2.45, 1.3375\sqrt{\rm W.u.}$ for neutron numbers 52–54 and $e^{(\rm B)} = 2.0325\sqrt{\rm W.u.}$ for 62. The fermion effective charge in $\hat{T}_{\rm f}(E2)$ is $e_{\rm f} = -2.361\sqrt{\rm W.u.}$, determined from a fit to the ground-state quadrupole moment of ^{93}Nb. For $\hat{T}_{\rm b}(M1)$ we use $g^{(\rm A)} = -0.21, -0.42\mu_N$ for neutron number 52–54 and zero otherwise, $g^{(\rm B)} = (Z/A)\mu_N$ and $\tilde{g}^{(\rm A)} = \tilde{g}^{(\rm B)} = 0$ $(-0.017\mu_N)$ for 52–56 (58–64). For $\hat{T}_{\rm f}(M1)$ we use $g_\ell = 1\mu_N$ and $g_s = 4.422\mu_N$.

The $B(E2; 7/2^+_1 \to J^+_{gs})$ and quadrupole moment of J^+_{gs} are shown in Figs. 2(b) and 2(c), respectively. These observables are related to the deformation, the order parameter of the QPT. Although the data are incomplete, one can still observe small (large) values of these observables below (above) neutron number 60, indicating an increase in deformation. The calculation reproduces well this trend and attributes it to a Type II QPT involving a jump between neutron number 58 and 60, from a weakly deformed A configuration, to a strongly deformed B configuration. Such a Type II scenario is supported also by the trend in the magnetic moments (μ_J) of the ground state, shown in Fig. 2(d), where both the data and the calculations show a constant value of μ_J for neutron numbers 52–58, and a drop to a lower value at 60, which persists for 60–64. This trend of approximately constant value for each range of neutron numbers suggests a corresponding constant mixing in the ground state wave function, in line with the calculated weak mixing before and after the crossing, shown in Fig. 2(a).

To identify a Type I QPT, involving shape changes within the intruder B configuration, we examine the individual structure of Nb isotopes at the end points of the region considered. Figure 3 displays the experimental and calculated levels in ^{93}Nb along with $E2$ and $M1$ transitions among them. The corresponding spectra of ^{92}Zr, the even-even core, are also shown with an assignment of each level L to the normal A or intruder B configurations, based on the analysis in Ref. [9], which also showed that the two configurations in ^{92}Zr are spherical or weakly deformed. It has long been known [50] that low-lying states of the A configuration in ^{93}Nb can be interpreted in a weak-coupling scheme, where the single-proton $\pi(1g_{9/2})$ state is coupled to spherical-vibrator states of the core. Specifically, for the $0^+_{1;\rm A}$ ground state of ^{92}Zr, this coupling yields the ground state $9/2^+_1$ of ^{93}Nb. For $2^+_{1;\rm A}$, it yields a quintuplet of states, $5/2^+_1, 7/2^+_1, 9/2^+_3, 11/2^+_1, 13/2^+_1$, whose

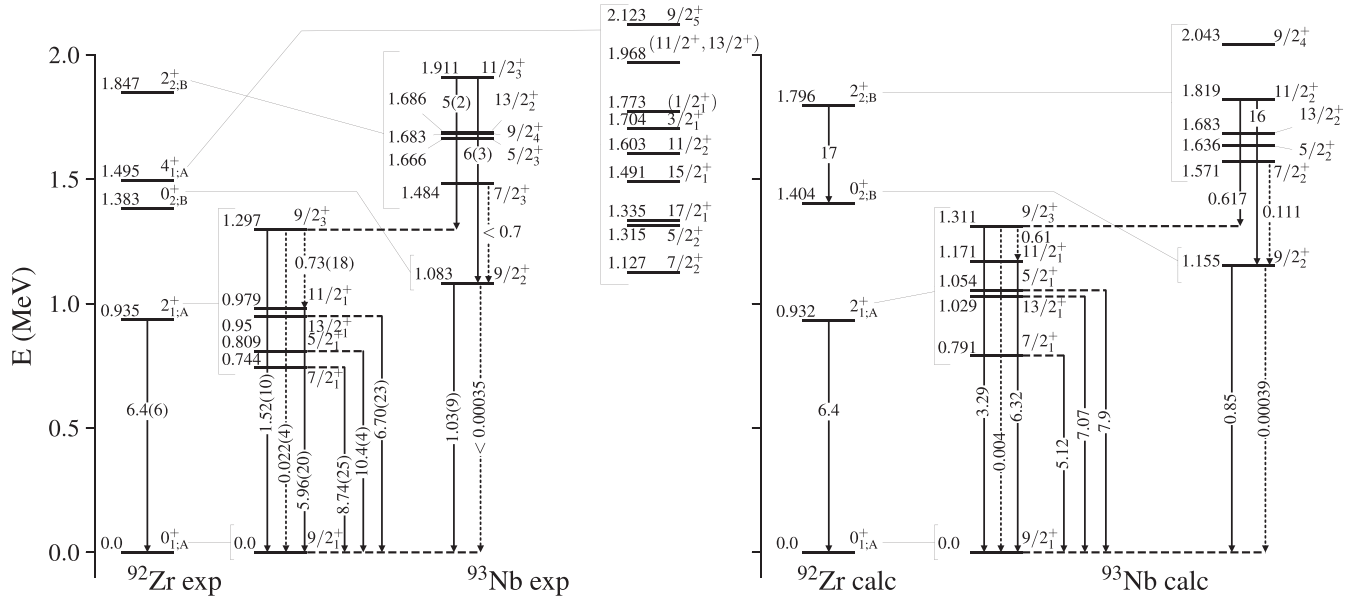

FIG. 3. Experimental (left) and calculated (right) energy levels in MeV, and $E2$ (solid arrows) and $M1$ (dashed arrows) transition rates in W.u., for ^{93}Nb and ^{92}Zr. Lines connect L levels in ^{92}Zr to sets of J levels in ^{93}Nb, indicating the weak coupling $(L \otimes \frac{9}{2})J$. Data taken from Refs. [42,49]. Note that the observed $4^+_{1;A}$ state in ^{92}Zr is outside the $N = 1$ model space.

"center of gravity" (CoG) [51], is 0.976 MeV, in agreement with the observed energy 0.935 MeV of 2^+_1 in ^{92}Zr. The $E2$ transitions from the quintuplet states to the ground state are comparable in magnitude to the $2^+_{1;A} \to 0^+_{1;A}$ transition in ^{92}Zr, except for $9/2^+_3$, whose decay is weaker. The corresponding $M1$ transitions are weak, while $M1$ transitions within states of the quintuplet are strong, as expected for weak-coupling to a spherical vibrator [16]. An octet of states built on $4^+_{1;A}$ can also be identified in the empirical spectrum of ^{93}Nb, with a CoG of 1.591 MeV, close to 1.495 MeV of $4^+_{1;A}$.

The weak-coupling scenario is also valid for states of the intruder B configuration in ^{93}Nb. As shown in Fig. 3, the coupling of $\pi(1g_{9/2})$ to the $0^+_{2;B}$ state in ^{92}Zr yields the excited $9/2^+_2$ state in ^{93}Nb. For $2^+_{2;B}$ it yields the quintuplet, $5/2^+_3, 7/2^+_3, 9/2^+_4, 11/2^+_3, 13/2^+_2$, whose CoG is 1.705 MeV, a bit lower than 1.847 MeV of $2^+_{2;B}$. The observed $E2$ rates 1.03(9) W.u. for $9/2^+_2 \to 9/2^+_1$, is close to the calculated value 0.85 W.u., but is smaller than the observed value 1.52(10) W.u. for $9/2^+_3 \to 9/2^+_1$, suggesting that $9/2^+_2$ is associated with the B configuration.

For ^{103}Nb, the yrast states shown in Fig. 4 are arranged in a $K = 5/2^+$ rotational band, with an established [53] Nilsson model assignment $5/2^+[422]$. The band members can be interpreted in the strong-coupling scheme, where a particle is coupled to an axially deformed core. The indicated states are obtained by coupling the $\pi(1g_{9/2})$ state to the ground band $(L = 0^+_1, 2^+_1, 4^+_1, \ldots)$ of ^{102}Zr, which is associated with the intruder B configuration. The calculations reproduce well the observed particle-rotor $J(J+1)$ splitting, as well as the $E2$ and $M1$ transitions within the band. Altogether, we see an evolution of structure from weak-coupling of a spherical shape in ^{93}Nb, to strong-coupling of a deformed shape in ^{103}Nb. Such shape changes within the B configuration (Type I QPT), superimposed on abrupt configuration crossing (Type II QPT), are the key defining feature of intertwined QPTs (IQPTs). Interestingly, the intricate IQPTs scenario, originally observed in the even-even Zr isotopes [8,9], persists in the adjacent odd-even Nb isotopes.

In conclusion, we have presented a general framework (IBFM-CM), allowing a quantitative description of configuration mixing and related QPTs in odd-mass nuclei. An application to the positive-parity states in odd-even Nb isotopes disclosed a Type II QPT (abrupt configuration crossing) accompanied by a Type I QPT (gradual shape evolution and transition from weak to strong coupling within the intruder configuration), thus demonstrating, for the first time,

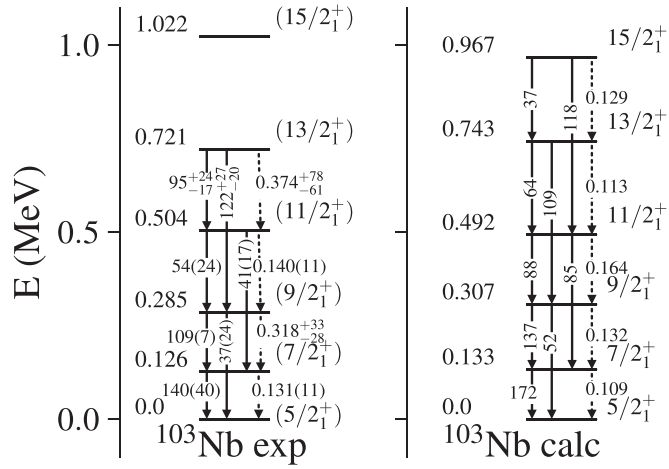

FIG. 4. Experimental (left) and calculated (right) energy levels in MeV, and $E2$ (solid arrows) and $M1$ (dashed arrows) transition rates in W.u., for ^{103}Nb. Data taken from Refs. [47,52].

IQPTs in odd-mass nuclei. The observed IQPTs in odd-*A* Nb isotopes echo the multiple QPTs previously found in the adjacent even-even Zr isotopes [8,9]. The results obtained motivate further experiments of non-yrast spectroscopy in such nuclei, as well as set the path for new investigations on multiple QPTs and coexistence in other Bose-Fermi systems.

This work is supported by the US-Israel Binational Science Foundation Grant No. 2016032. N.G. acknowledges support by the Israel Academy of Sciences of a Postdoctoral Fellowship Program in Nuclear Physics. We thank P. Van Isacker for providing his IBFM code, which served as a basis for the IBFM-CM computer program.

[1] R. Gilmore and D. H. Feng, Phys. Lett. B **76**, 26 (1978).
[2] R. Gilmore, J. Math. Phys. **20**, 891 (1979).
[3] *Understanding Quantum Phase Transitions*, edited by L. Carr (CRC Press, Boca Raton, FL, 2011).
[4] A. E. L. Dieperink, O. Scholten, and F. Iachello, Phys. Rev. Lett. **44**, 1747 (1980).
[5] P. Cejnar, J. Jolie, and R. F. Casten, Rev. Mod. Phys. **82**, 2155 (2010).
[6] A. Frank, P. Van Isacker, and F. Iachello, Phys. Rev. C **73**, 061302(R) (2006).
[7] K. Heyde and J. L. Wood, Rev. Mod. Phys. **83**, 1467 (2011).
[8] N. Gavrielov, A. Leviatan, and F. Iachello, Phys. Rev. C **99**, 064324 (2019).
[9] N. Gavrielov, A. Leviatan, and F. Iachello, Phys. Rev. C **105**, 014305 (2022).
[10] R. F. Casten, Prog. Part. Nucl. Phys. **62**, 183 (2009).
[11] F. Iachello, Riv. Nuovo Cimento **34**, 617 (2011).
[12] L. Fortunato, Prog. Part. Nucl. Phys. **121**, 103891 (2021).
[13] E. Caurier, G. Martínez-Pinedo, F. Nowacki, A. Poves, and A. P. Zuker, Rev. Mod. Phys. **77**, 427 (2005).
[14] B. Bally, B. Avez, M. Bender, and P.-H. Heenen, Phys. Rev. Lett. **113**, 162501 (2014).
[15] O. Scholten and N. Blasi, Nucl. Phys. A **380**, 509 (1982).
[16] F. Iachello and P. Van Isacker, *The Interacting Boson-Fermion Model* (Cambridge University Press, Cambridge, UK, 1991).
[17] D. Petrellis, A. Leviatan, and F. Iachello, Ann. Phys. **326**, 926 (2011).
[18] J. Jolie, S. Heinze, P. Van Isacker, and R. F. Casten, Phys. Rev. C **70**, 011305(R) (2004).
[19] C. E. Alonso, J. M. Arias, L. Fortunato, and A. Vitturi, Phys. Rev. C **72**, 061302(R) (2005).
[20] C. E. Alonso, J. M. Arias, and A. Vitturi, Phys. Rev. C **75**, 064316 (2007).
[21] C. E. Alonso, J. M. Arias, L. Fortunato, and A. Vitturi, Phys. Rev. C **79**, 014306 (2009).
[22] M. Böyükata, C. E. Alonso, J. M. Arias, L. Fortunato, and A. Vitturi, Phys. Rev. C **82**, 014317 (2010).
[23] F. Iachello, A. Leviatan, and D. Petrellis, Phys. Lett. B **705**, 379 (2011).
[24] M. Böyükata, C. E. Alonso, J. M. Arias, L. Fortunato, and A. Vitturi, Symmetry **13**, 215 (2021).
[25] K. Nomura, T. Nikšić, and D. Vretenar, Phys. Rev. C **93**, 054305 (2016).
[26] K. Nomura, T. Nikšić, and D. Vretenar, Phys. Rev. C **94**, 064310 (2016).
[27] K. Nomura, T. Nikšić, and D. Vretenar, Phys. Rev. C **102**, 034315 (2020).
[28] S. Quan, Z. P. Li, D. Vretenar, and J. Meng, Phys. Rev. C **97**, 031301(R) (2018).
[29] P. Spagnoletti, G. Simpson, S. Kisyov, D. Bucurescu, J.-M. Régis, N. Saed-Samii, A. Blanc, M. Jentschel, U. Köster, P. Mutti, T. Soldner, G. de France, C. A. Ur, W. Urban, A. M. Bruce, C. Bernards, F. Drouet, L. M. Fraile, L. P. Gaffney, D. G. Ghiță *et al.*, Phys. Rev. C **100**, 014311 (2019).
[30] F. Boulay, G. S. Simpson, Y. Ichikawa, S. Kisyov, D. Bucurescu, A. Takamine, D. S. Ahn, K. Asahi, H. Baba, D. L. Balabanski, T. Egami, T. Fujita, N. Fukuda, C. Funayama, T. Furukawa, G. Georgiev, A. Gladkov, M. Hass, K. Imamura, N. Inabe *et al.*, Phys. Rev. Lett. **124**, 112501 (2020).
[31] P. D. Duval and B. R. Barrett, Phys. Lett. B **100**, 223 (1981).
[32] P. D. Duval and B. R. Barrett, Nucl. Phys. A **376**, 213 (1982).
[33] M. Sambataro and G. Molnár, Nucl. Phys. A **376**, 201 (1982).
[34] J. E. García-Ramos and K. Heyde, Phys. Rev. C **89**, 014306 (2014).
[35] J. E. García-Ramos and K. Heyde, Phys. Rev. C **92**, 034309 (2015).
[36] K. Nomura, R. Rodríguez-Guzmán, and L. M. Robledo, Phys. Rev. C **94**, 044314 (2016).
[37] A. Leviatan, N. Gavrielov, J. E. García-Ramos, and P. Van Isacker, Phys. Rev. C **98**, 031302(R) (2018).
[38] J. E. García-Ramos and K. Heyde, Phys. Rev. C **100**, 044315 (2019).
[39] E. Maya-Barbecho and J. E. García-Ramos, Phys. Rev. C **105**, 034341 (2022).
[40] J. Barea and F. Iachello, Phys. Rev. C **79**, 044301 (2009).
[41] C. M. Baglin, Nucl. Data Sheets **114**, 1293 (2013).
[42] C. M. Baglin, Nucl. Data Sheets **112**, 1163 (2011).
[43] S. Basu, G. Mukherjee, and A. Sonzogni, Nucl. Data Sheets **111**, 2555 (2010).
[44] N. Nica, Nucl. Data Sheets **111**, 525 (2010).
[45] E. Browne and J. Tuli, Nucl. Data Sheets **145**, 25 (2017).
[46] R. Rodríguez-Guzmán, P. Sarriguren, and L. M. Robledo, Phys. Rev. C **83**, 044307 (2011).
[47] D. De Frenne, Nucl. Data Sheets **110**, 2081 (2009).
[48] B. Cheal, K. Baczynska, J. Billowes, P. Campbell, F. C. Charlwood, T. Eronen, D. H. Forest, A. Jokinen, T. Kessler, I. D. Moore, M. Reponen, S. Rothe, M. Rüffer, A. Saastamoinen, G. Tungate, and J. Äystö, Phys. Rev. Lett. **102**, 222501 (2009).
[49] J. N. Orce, J. D. Holt, A. Linnemann, C. J. McKay, C. Fransen, J. Jolie, T. T. S. Kuo, S. R. Lesher, M. T. McEllistrem, N. Pietralla, N. Warr, V. Werner, and S. W. Yates, Phys. Rev. C **82**, 044317 (2010).

[50] I. J. van Heerden, W. R. McMurray, and R. Saayman, Z. Phys. **260**, 9 (1973).
[51] R. D. Lawson and J. L. Uretsky, Phys. Rev. **108**, 1300 (1957).
[52] T. W. Hagen, A. Görgen, W. Korten, L. Grente, M.-D. Salsac, F. Farget, I. Ragnarsson, T. Braunroth, B. Bruyneel, I. Celikovic, E. Clément, G. de France, O. Delaune, A. Dewald, A. Dijon, M. Hackstein, B. Jacquot, J. Litzinger, J. Ljungvall, C. Louchart *et al.*, Phys. Rev. C **95**, 034302 (2017).
[53] M. A. C. Hotchkis, J. L. Durell, J. B. Fitzgerald, A. S. Mowbray, W. R. Phillips, I. Ahmad, M. P. Carpenter, R. V. F. Janssens, T. L. Khoo, E. F. Moore, L. R. Morss, Ph. Benet, and D. Ye, Nucl. Phys. A **530**, 111 (1991).